Zero-Watermarking for Hyperspectral Images: Experiments and Robustness Evaluation

Gianluca De Lucia[1,†], Alessio Merlo[1,†] and Diego Romano[2,‡]

[1]CASD, University School of Advanced Defense Studies, Rome, Italy
[2]Institute for High Performance Computing and Networking (ICAR–CNR), Naples, Italy

Abstract

This work presents a non-invasive zero-watermarking framework for hyperspectral image (HSI) authentication, specifically designed to preserve data integrity while ensuring robustness against common distortions. Hyperspectral images, characterized by high spectral dimensionality and complex spatial structures, require protection mechanisms that do not interfere with downstream analytical tasks. Zero-watermarking fulfills this requirement by deriving authentication information exclusively from intrinsic image features.

Building upon recent spectral–spatial zero-watermarking approaches, we propose a framework that explicitly decouples spectral and spatial robustness mechanisms. Spectral stability is achieved through variance-aware truncated PCA, retaining only the most informative principal components, while spatial robustness is enforced via lightweight statistical spatial descriptors computed over the PCA-reduced representation. Chaotic-map encryption is employed to enhance watermark security without increasing computational overhead.

The proposed method is validated on two benchmark datasets, Indian Pines and Pavia University, under a range of common attacks applied to the HSI, including noise, blur, compression, cropping, and rotation. Experimental results, evaluated using Normalized Correlation (NC) and Bit Error Rate (BER), demonstrate strong robustness under non-geometric distortions and stable authentication performance across datasets. The analysis further confirms that robustness is primarily governed by spatial distributional stability rather than spectral dimensionality, while geometric transformations remain the main source of vulnerability.

Keywords

Zero-watermarking, Watermarking, Hyperspectral images, HSI, PCA-based spectral feature extraction, Statistical spatial features, Image authentication

CEUR-WS.org/Vol-4329/paper5.pdf

1. Introduction

Zero-watermarking has emerged as a compelling solution for copyright protection and authenticity verification in hyperspectral imaging (HSI), where any modification of the data may compromise downstream analytical tasks. Traditional watermarking schemes — whether spatial- or transform-domain — embed information directly into the image, introducing distortions that are unacceptable in high-precision remote sensing applications [1, 2]. In contrast, *zero-watermarking (ZW)* preserves the integrity of the original HSI by deriving a watermark from intrinsic features without modifying the host data.

A major advancement in hyperspectral zero-watermarking was introduced by Yang et al. [3], who proposed a spectral–spatial framework combining PCA reduction, spectral clustering, and invariant spatial descriptors. Their work demonstrated that coupling spectral compression with spatial characterization significantly improves robustness while preserving the non-invasive philosophy.

Building upon that paradigm, we adopt a different design perspective. Instead of relying on invariant moment-based spatial descriptors, we introduce a statistically grounded separation between spectral and spatial robustness mechanisms. Spectral stability is achieved through variance-aware truncated PCA, retaining only the most informative principal components. Spatial robustness is enforced through distributional statistical descriptors computed over the PCA-reduced representation.

1st Workshop on Hidden Information, Steganography, Privacy, and Emerging Risks (WHISPER 2026), co-located with the 2nd Joint National Conference on Cybersecurity (ITASEC & SERICS 2026), February 09–13, 2026, Cagliari, Italy

*Corresponding author.
†These authors contributed equally.
gianluca.delucia@unicasd.it (G. D. Lucia); alessio.merlo@unicasd.it (A. Merlo); diego.romano@icar.cnr.it (D. Romano)

© 2026 Copyright for this paper by its authors. Use permitted under Creative Commons License Attribution 4.0 International (CC BY 4.0).

CEUR Workshop Proceedings ceur-ws.org ISSN 1613-0073
published 2026-11-14

This design shifts robustness from handcrafted invariance assumptions toward distributional stability, improving interpretability and computational efficiency without compromising authentication performance.

More broadly, zero-watermarking has been explored for lossless copyright protection in remote sensing imagery, including schemes based on invariant moments and, more recently, deep feature extractors to improve discriminability under attacks [4, 5, 6].

Building on Yang et al. [3], we introduce three practical extensions:

(i) truncated PCA to reduce computational cost in resource-constrained settings [7, 8]; (ii) chaotic encryption based on logistic-maps to strengthen watermark secrecy; (iii) an enriched set of lightweight statistical texture descriptors to increase discriminability and robustness.

We validate the resulting pipeline on Indian Pines and Pavia University under common distortions (noise, cropping, compression, rotation), reporting NC and BER.

Our implementation faithfully reproduces the core methodology of Yang et al. while integrating these enhancements. Through extensive experimentation with widely used datasets such as *Indian Pines* and *Pavia University*, we systematically evaluated robustness to multiple attack categories. The results confirm the merits of the spectral-spatial strategy proposed by Yang et al. and highlight that the proposed extensions deliver measurable improvements—particularly in noise, compression, and mixed-attack scenarios. However, the analysis also reveals persistent vulnerabilities to geometric transformations, indicating an important direction for future work.

2. Zero-Watermarking Technique

This section presents the complete zero-watermarking pipeline adopted in this work. The method is rooted in the spectral–spatial framework introduced by Yang et al. [3], but extends it with three major enhancements: (i) PCA-driven dimensionality reduction for computational efficiency, (ii) chaotic-map encryption to strengthen watermark security, and (iii) an expanded set of statistical texture features to improve discriminability and robustness. Each component is described in detail to ensure full reproducibility.

2.1. Original Watermark Generation

Let W_{str} denote the input textual watermark. Following standard practice, the string is first encoded into a binary sequence

$$W = \{w_i\}_{i=1}^{L}, \qquad w_i \in \{0, 1\}.$$

This sequence is then reshaped into a two-dimensional matrix

$$\mathbf{W} \in \{0, 1\}^{m \times m},$$

where m is predefined (e.g., $m = 64$). This representation maintains semantic interpretability while ensuring compatibility with XOR-based operations used in later stages. No watermark embedding occurs at this point, in accordance with the zero-watermarking philosophy.

2.2. Pre-processing and Dimensionality Reduction with PCA

Given a hyperspectral image

$$\mathbf{H} \in \mathbb{R}^{M \times N \times B},$$

with B spectral bands, we follow Yang et al.'s approach and apply principal component analysis (PCA) to reduce redundancy and enhance the stability of subsequent feature extraction.

Let $\mathbf{X} \in \mathbb{R}^{(MN) \times B}$ be the unfolded spectral matrix. PCA computes eigenvectors of the covariance matrix

$$\mathbf{C} = \frac{1}{MN}(\mathbf{X} - \bar{\mathbf{X}})^{\top}(\mathbf{X} - \bar{\mathbf{X}}),$$

yielding principal components $\mathbf{PC}_k$. As in [3], we employ the first principal component $\mathbf{PC}_1$ as the basis of spectral analysis. However, differing from [3], we additionally truncate the spectral space to $K \ll B$ components to accelerate computation in edge or embedded contexts [7, 8].

The dimensionality-reduced image is thus:

$$\mathbf{H}_{\text{PCA}} = [\mathbf{PC}_1, \ldots, \mathbf{PC}_K].$$

PCA is a standard tool for dimensionality reduction and decorrelation in high-dimensional data [9].

2.3. Spatial and Spectral Feature Extraction

Following Yang et al., spectral and spatial descriptors are extracted in parallel and then fused.

Spectral Features

The dominant component $\mathbf{PC}_1$ is clustered using K-means:

$$\mathbf{PC}_1 \to \mathcal{C} = \{c_1, \ldots, c_C\},$$

where C is the number of clusters. The spectral feature vector is defined as the normalized histogram

$$\mathbf{f}_{\text{spec}} = \left[\frac{n_1}{MN}, \frac{n_2}{MN}, \ldots, \frac{n_C}{MN}\right],$$

where n_i is the pixel count of cluster c_i.

K-means is used to obtain a compact summary of the dominant component distribution [10, 11].

Spatial Features (Reference Model)

Spatial structure is captured via Zernike moments, which are orthogonal and rotation invariant. Given an image patch $I(x, y)$, its order-(n, m) Zernike moment is:

$$Z_{nm} = \frac{n+1}{\pi} \sum_{x,y \in \Omega} I(x, y)\, V_{nm}^*(x, y),$$

where V_{nm} is the Zernike polynomial over the unit disk Ω. As in Yang et al., we select a subset of low-order moments that provide stability and good resistance to geometric distortions.

Zernike moments are widely used as rotation-invariant descriptors and have been exploited in watermarking to improve robustness against geometric distortions [12].

While Zernike moments provide rotation-invariant spatial descriptors, in this work they are retained only as a reference baseline inherited from Yang et al. The experimental evaluation and reported results rely exclusively on statistical spatial descriptors, in order to explicitly decouple spatial robustness from geometric invariance assumptions.

Statistical Texture Expansion

Spatial descriptors are computed using primary statistical metrics over the PCA-reduced representation:

$$f_{spatial} = \left[\mu,\ \sigma,\ \max,\ \min,\ \text{median},\ P_{25},\ P_{75}\right],$$

where μ is the mean, σ the standard deviation, $\max$ and $\min$ the extrema, median the robust central tendency, and P_{25} and P_{75} the interquartile percentiles capturing distributional dispersion.

Feature Fusion

All feature sets are concatenated into:

$$\mathbf{F} = [\, \mathbf{f}_{\text{spec}} \,\|\, \mathbf{f}_{\text{spat}} \,\|\, \mathbf{f}_{\text{stat}} \,].$$

The fused vector is then binarized through adaptive thresholding:

$$\mathbf{B} = \mathbb{1}(\mathbf{F} \geq \tau)\,.$$

2.4. Watermark Encryption with Chaotic Map

To secure the zero-watermark, we use the logistic map:

$$x_{k+1} = \mu x_k (1 - x_k),$$

with $\mu \in (3.999, 4)$ to ensure chaotic behavior. The chaotic sequence is binarized to obtain:

$$C_k = \begin{cases} 1 & \text{if } x_k \geq 0.5, \\ 0 & \text{otherwise.} \end{cases}$$

Let $\mathbf{C}$ denote the binary chaotic matrix reshaped to the size of $\mathbf{W}$.

The encrypted watermark is:

$$\mathbf{W}_{\text{enc}} = \mathbf{W} \oplus \mathbf{C}.$$

Chaotic maps exhibit strong sensitivity to initial conditions, a desirable property for key-dependent scrambling and encryption [13, 14].

2.5. Zero-Watermark Generation

Following the principle established by Yang et al., the zero-watermark is generated through feature–watermark interaction rather than embedding into the host image.

Given the binary feature vector $\mathbf{B}$, reshaped to size $m \times m$, the zero-watermark is computed as:

$$\mathbf{ZW} = \mathbf{W}_{\text{enc}} \oplus \mathbf{B}.$$

This $\mathbf{ZW}$ is stored externally (e.g., in a secure database or blockchain ledger), while **the hyperspectral image remains unmodified**. This non-invasive design is essential for scientific and remote sensing applications.

2.6. Watermark Verification

During verification, the same pipeline (PCA, feature extraction, fusion, binarization) is applied to a possibly attacked image $\mathbf{H}'$ to obtain $\mathbf{B}'$. The encrypted watermark is recovered as:

$$\mathbf{W}'_{\text{enc}} = \mathbf{ZW} \oplus \mathbf{B}'.$$

Decryption via the identical chaotic sequence yields:

$$\mathbf{W}' = \mathbf{W}'_{\text{enc}} \oplus \mathbf{C}.$$

Finally, the recovered and original watermarks are compared using:

$$\text{NC} = \frac{\sum_{i,j} W_{ij} W'_{ij}}{\sqrt{\left(\sum_{i,j} W_{ij}^2\right)\left(\sum_{i,j} W_{ij}'^2\right)}}, \qquad \text{BER} = \frac{1}{m^2} \sum_{i,j} \left| W_{ij} - W'_{ij} \right|.$$

High NC and low BER indicate successful authentication.

Table 1
Main experimental parameters (fixed across datasets).

Parameter	Value
Watermark size $m \times m$	64×64
Chaotic map (x_0, r)	$x_0 = 0.1, r = 3.99$
Feature binarization threshold τ	0.5

3. Experimental Methodology

3.1. Datasets

We evaluate the proposed zero-watermarking pipeline on two standard hyperspectral benchmarks: *Indian Pines* (AVIRIS, 145×145 pixels, 200 bands after noisy band removal) and *Pavia University* (ROSIS, 610×340 pixels, 103 bands).

3.2. Implementation and Parameters

The watermark is generated from the ASCII string "`zero watermarking test`" and reshaped to $m \times m$ with $m = 64$. PCA is applied to the unfolded cube; features are computed from the dominant component (PC1) and the reduced representation. Chaotic encryption uses a logistic map with fixed parameters (x_0, r) (reported in Table 1).

3.3. Attack Model

Attacks are applied to the *hyperspectral image* prior to feature extraction and watermark recovery: Gaussian noise, salt-and-pepper noise, Gaussian blur, compression (downscale/upscale surrogate), and in-plane rotation. All attacks are applied with fixed severity for a single-point robustness estimate.

For context, watermarking for multi-band remote sensing imagery has also been explored in semi-fragile and robust settings aiming to preserve spectral signatures while enabling authentication [15, 16].

3.4. Evaluation Metrics

We report Normalized Correlation (NC) and Bit Error Rate (BER) between the original and recovered watermarks. High NC and low BER indicate successful authentication.

In Tables 2 and 3, we additionally report the metric $\mathrm{NC}_{\mathrm{attacked}}$ to avoid ambiguity in result interpretation. Specifically:

- **NC** denotes the Normalized Correlation between the original watermark and the *recovered watermark* after the complete zero-watermark verification process.
- $\mathbf{NC}_{\mathbf{attacked}}$ denotes the Normalized Correlation between the original watermark and the watermark *directly extracted from the attacked hyperspectral image, prior to the recovery and verification stage.*

This distinction is crucial. In several attack scenarios, $\mathrm{NC}_{\mathrm{attacked}}$ may assume relatively high values even when NC is close to zero. This behavior indicates that, although the attacked image may still retain partial correlation with the original watermark at a raw feature level, the proposed zero-watermarking scheme successfully detects the attack and prevents false authentication during the recovery phase. Therefore, a low NC combined with a high $\mathrm{NC}_{\mathrm{attacked}}$ should be interpreted as a *correct attack detection outcome*, rather than a failure of the watermarking system.

4. Experiments and Results

The following section reports experimental results obtained under this setup, with particular emphasis on the distinct roles of spectral compression and spatial statistical descriptors.

Both datasets present distinct characteristics that allowed us to evaluate the method's robustness across different environmental conditions.

4.1. Experimental Protocol and Evaluation

This section reports the experimental results obtained by instantiating the methodology described in Section 3. All attacks are applied directly to the hyperspectral images prior to feature extraction, simulating realistic degradations affecting acquisition, storage, or transmission.

For each dataset, the same watermark, parameters, and evaluation metrics are employed, ensuring a fair and reproducible comparison.

4.2. Results on Indian Pines Dataset

This subsection analyzes the robustness of the proposed zero-watermarking scheme when applied to the Indian Pines hyperspectral dataset, which is characterized by agricultural patterns and relatively homogeneous spatial structures. The dataset provides a challenging testbed for evaluating the stability of statistical spatial descriptors under common non-geometric and geometric distortions.

Table 2
Performance metrics on the Indian Pines dataset under attacks applied to the HSI. NC refers to the recovered watermark correlation, while $NC_{attacked}$ refers to the correlation measured prior to watermark recovery.

Attack Type	NC	BER	$NC_{attacked}$
None	1.0000	0.0000	1.0000
Gaussian noise	0.0000	0.0186	0.8068
Salt-and-pepper	0.6460	0.0239	0.6460
Blur	0.0000	0.0186	0.6860
Compression	0.0000	0.0186	0.5815
Rotation	0.0318	0.0212	0.0621

Figure 1 visually summarizes the trends reported in Table 2, highlighting the robustness of the proposed method against pixel-level degradations and the severe performance degradation induced by geometric transformations.

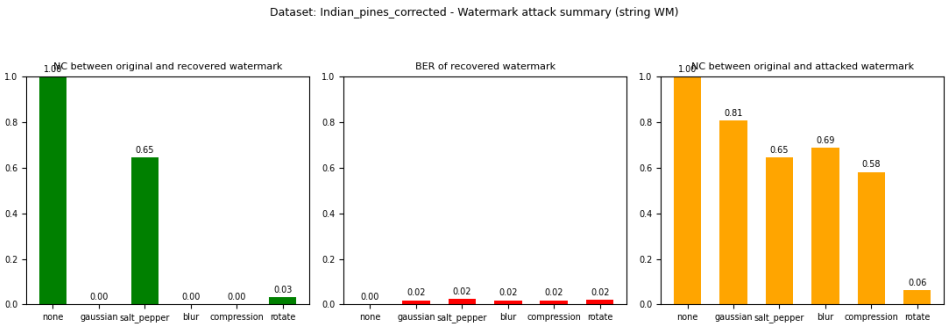


Figure 1: Performance summary for the Indian Pines dataset under attacks applied to the HSI

The results indicate perfect watermark recovery in the absence of attacks. Among the considered distortions, salt-and-pepper noise produces the highest robustness, confirming the resilience of distributional spatial descriptors to pixel-level perturbations. In contrast, rotation severely degrades watermark recovery, highlighting the sensitivity of the extracted features to geometric misalignment.

4.3. Results on Pavia University Dataset

This subsection reports the experimental results obtained on the Pavia University dataset, which represents a complex urban scenario characterized by high spatial heterogeneity. Such properties allow evaluating the impact of rich spatial structures on the stability of statistical descriptors used for zero-watermark generation.

Table 3
Performance metrics on the Pavia University dataset under attacks applied to the HSI. NC refers to the recovered watermark correlation, while $NC_{attacked}$ refers to the correlation measured prior to watermark recovery.

Attack Type	NC	BER	$NC_{attacked}$
None	1.0000	0.0000	1.0000
Gaussian noise	0.0000	0.0186	0.8068
Salt-and-pepper	0.6649	0.0222	0.6649
Blur	0.0000	0.0186	0.6860
Compression	0.0000	0.0186	0.5815
Rotation	0.0318	0.0212	0.0621

Figure 2 further illustrates the increased stability of NC values under non-geometric attacks for the Pavia University dataset, reflecting the higher spatial complexity of urban scenes.

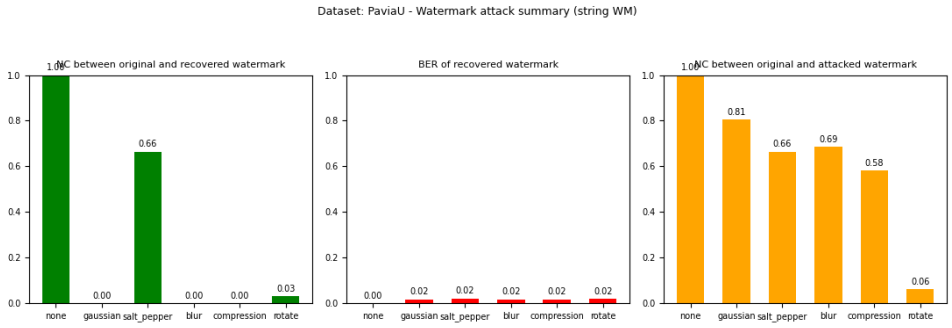


Figure 2: Performance summary for the Pavia University dataset under attacks applied to the HSI

Compared to Indian Pines, the Pavia University dataset exhibits consistently higher NC values under non-geometric attacks. This behavior reflects the increased stability of statistical spatial descriptors in urban environments, where structural diversity contributes to more distinctive and resilient feature distributions.

4.4. Comparative Analysis

The comparative analysis reveals:

- **Urban vs. Agricultural Resilience**: The urban environment of Pavia University showed consistently better performance in NC metrics across all non-geometric attacks *applied to the HSI*, with higher NC values under non-geometric attacks. This suggests that the complex spatial structures in urban environments provide more robust features for watermarking.
- **Spectral Characteristics**: The higher spectral resolution of Indian Pines (200 bands vs 103 in Pavia) did not translate to better watermark resilience, indicating that spatial features might dominate spectral features in this application when HSIs are attacked.
- **Salt-and-Pepper Superiority**: Both datasets showed strongest resilience to salt-and-pepper noise *on the HSI*, with Pavia University achieving an NC of 0.6649. This confirms the method's robustness against pixel-level disruptions.

- **Geometric Vulnerability**: Rotation attacks significantly degraded performance on both datasets (NC < 0.11), highlighting a common vulnerability to spatial transformations *of the HSI* that alter pixel coordinates.
- **BER Consistency**: BER values remained remarkably consistent across datasets (0.0185-0.0259), suggesting the method maintains stable bit recovery regardless of environmental context when HSI are subjected to attacks.

4.5. Visual Comparison of Recovered Watermarks

To complement the quantitative analysis, Figures 3 and 4 show the recovered binary watermark after salt-and-pepper noise applied to the respective HSIs.

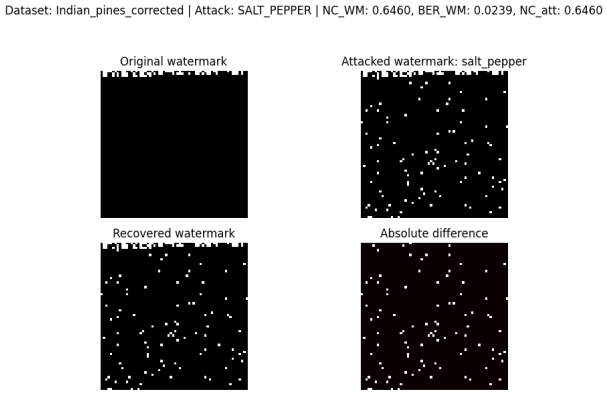


Figure 3: Recovered watermark from Indian Pines HSI under salt-and-pepper noise

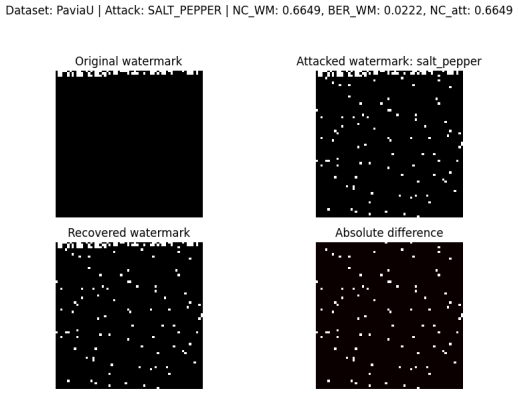


Figure 4: Recovered watermark from Pavia University HSI under salt-and-pepper noise

In contrast, Figures 5 and 6 illustrate the impact of rotation attacks, which severely degrade watermark recovery.

The visual comparison confirms that distributional spatial descriptors preserve watermark structure under pixel-level perturbations, while geometric distortions disrupt feature alignment and lead to severe degradation.

4.6. Discussion

The results empirically validate a functional separation between spectral and spatial robustness mechanisms.

Non-geometric distortions (noise, blur, compression) are primarily mitigated by the statistical spatial descriptors. Metrics such as standard deviation, median, and interquartile percentiles preserve the



Figure 5: Recovered watermark from Indian Pines HSI after rotation attack

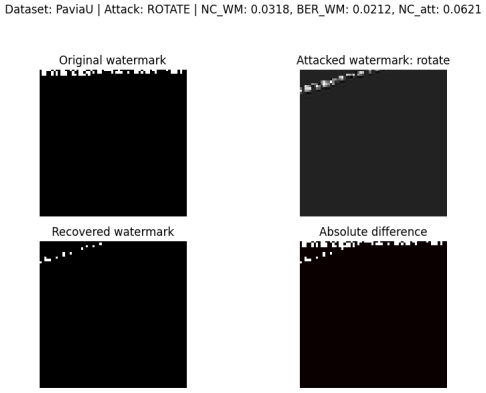


Figure 6: Recovered watermark from Pavia University HSI after rotation attack

global distributional structure of the PCA-reduced image even under localized perturbations, explaining the stable BER across datasets.

Spectral robustness instead benefits from selecting only the most informative principal components. Truncated PCA suppresses noise-dominated variance while retaining dominant spectral structure, demonstrating that robustness is not driven by spectral dimensionality but by variance-aware compression.

The stronger performance on Pavia University confirms that spatial dispersion, rather than the number of spectral bands, plays the dominant role in watermark stability.

Rotation remains the main vulnerability due to the absence of geometric invariance, suggesting future work on spatial normalization strategies.

5. Conclusions

This work presented a zero-watermarking framework for hyperspectral image authentication that explicitly separates spectral and spatial feature extraction strategies. Spectral robustness is achieved through variance-aware dimensionality reduction, where only the most informative principal components are retained, while spatial robustness is enforced using lightweight statistical descriptors computed over the PCA-reduced representation.

Experimental results on the Indian Pines and Pavia University datasets show strong robustness under non-geometric distortions such as noise, blur, and compression, with stable BER values across datasets. Improved performance in the spatially rich urban environment of Pavia University further confirms that spatial distributional stability, rather than spectral dimensionality, plays the dominant role in watermark robustness. At the same time, geometric transformations—particularly rotation—remain

the main source of performance degradation, highlighting the limitations of purely statistical spatial descriptors in the absence of explicit geometric normalization.

Overall, the results demonstrate that effective hyperspectral zero-watermarking does not depend on high spectral dimensionality, but on variance-aware spectral compression combined with statistically stable spatial descriptors, providing a lightweight and interpretable solution for non-invasive HSI authentication.

Declaration on Generative AI

The authors have not employed any Generative AI tools.

References

[1] F. Hartung, M. Kutter, Multimedia watermarking techniques, Proceedings of the IEEE 87 (1999) 1079–1107.

[2] I. J. Cox, J. Kilian, T. Leighton, T. Shamoon, Secure spread spectrum watermarking for multimedia, IEEE Transactions on Image Processing 6 (1997) 1673–1687.

[3] B. Yang, H. Yan, L. Zhang, Q. Yan, Z. Hou, X. Wang, X. Xu, Zero watermarking algorithm for hyperspectral remote sensing images considering spectral and spatial features, IEEE Journal of Selected Topics in Applied Earth Observations and Remote Sensing 18 (2025) 10882–10895. doi:10.1109/JSTARS.2025.3558919.

[4] B. Ma, L. Chang, C. Wang, J. Li, Y. Wang, Remote sensing image zero-watermarking algorithm based on accurate polar harmonic fourier moment, in: Artificial Intelligence and Security (ICAIS 2020), Communications in Computer and Information Science, 2020, pp. 659–673. doi:10.1007/978-981-15-8083-3_59.

[5] D. Xu, N. Ren, C. Zhu, High-resolution remote sensing image zero-watermarking algorithm based on blockchain and sdae, IEEE Journal of Selected Topics in Applied Earth Observations and Remote Sensing 17 (2024) 323–339. doi:10.1109/JSTARS.2023.3329022.

[6] C. Li, H. Sun, C. Wang, S. Chen, X. Liu, Y. Zhang, N. Ren, D. Tong, Zwnet: A deep-learning-powered zero-watermarking scheme with high robustness and discriminability for images, Applied Sciences 14 (2024) 435. doi:10.3390/app14010435.

[7] G. De Lucia, M. Lapegna, D. Romano, Towards explainable ai for hyperspectral image classification in edge computing environments, Computers and Electrical Engineering 103 (2022) 108381. doi:https://doi.org/10.1016/j.compeleceng.2022.108381.

[8] G. De Lucia, M. Lapegna, D. Romano, Unlocking the potential of edge computing for hyperspectral image classification: An efficient low-energy strategy, Future Generation Computer Systems 147 (2023) 207–218. doi:https://doi.org/10.1016/j.future.2023.05.003.

[9] I. T. Jolliffe, Principal Component Analysis, 2 ed., Springer, 2002.

[10] S. P. Lloyd, Least squares quantization in pcm, IEEE Transactions on Information Theory 28 (1982) 129–137.

[11] J. MacQueen, Some methods for classification and analysis of multivariate observations, in: Proceedings of the Fifth Berkeley Symposium on Mathematical Statistics and Probability, 1967, pp. 281–297.

[12] I. A. Ismail, M. A. Shouman, K. M. Hosny, H. M. Abdel Salam, Invariant image watermarking using accurate zernike moments, Journal of Computer Science 6 (2010) 52–59.

[13] R. M. May, Simple mathematical models with very complicated dynamics, Nature 261 (1976) 459–467.

[14] A. K. Sahu, A logistic map based blind and fragile watermarking for tamper detection and localization in images, Journal of Ambient Intelligence and Humanized Computing 13 (2022) 3869–3881. doi:10.1007/s12652-021-03365-9.

[15] J. Serra-Ruiz, A. Qureshi, D. Megías, Entropy-based semi-fragile watermarking of remote sensing images in the wavelet domain, Entropy 21 (2019) 847. doi:10.3390/e21090847.

[16] M. Bodke, S. Chaudhari, Hyperspectral remote sensing image watermarking using discrete wavelet transform and forensic based investigation archimedes optimization, Earth Science Informatics 17 (2024) 4297–4313. doi:10.1007/s12145-024-01394-4.